Available online at www.sciencedirect.com
ScienceDirect
Applied Catalysis B: Environmental 81 (2008) 132–140
APPLIED CATALYSIS B: ENVIRONMENTAL
www.elsevier.com/locate/apcatb

Structure and reactivity of plasma treated Ni/Al_2O_3 catalyst for CO_2 reforming of methane

Xinli Zhu [a,1], Peipei Huo [a], Yue-ping Zhang [b], Dang-guo Cheng [a], Chang-jun Liu [a,*]

[a] *Key Laboratory for Green Chemical Technology of Ministry of Education, School of Chemical Engineering and Technology, Tianjin 30072, China*
[b] *Department of Chemistry, Tianjin University, Tianjin 30072, China*

Received 19 July 2007; received in revised form 15 October 2007; accepted 28 November 2007
Available online 15 December 2007

Abstract

The glow discharge plasma treated Ni/Al_2O_3 catalyst showed an excellent anti-coke property for CO_2 reforming of methane. Characterizations using X-ray powder diffraction (XRD), X-ray photoelectron spectroscopy (XPS), temperature programmed reduction (TPR), transmission electron microscopy (TEM), and CO adsorbed infrared spectroscopy (IR) were conducted to investigate the structure and reactivity of the plasma treated Ni/Al_2O_3 catalyst for CO_2 reforming of methane. It confirms that the plasma treatment of Ni precursor at room temperature followed by calcination thermally has a significant influence on the surface characteristics of the active phase. The plasma treated catalyst contains high concentration of close packed plane with improved Ni dispersion and enhanced Ni-alumina interaction, which lead to high catalytic activity and excellent resistance to formations of filamentous carbon and encapsulating carbon.

Keywords: Dry reforming; Methane; Nickel; Synthesis gas

1. Introduction

Carbon dioxide reforming of methane (or dry reforming) to synthesis gas (1) has received great attention in the past two decades [1–10] for a number of reasons. Firstly, the greenhouse effect has become more serious recently. As early as in 1992, 65% of global warming was estimated to come from emission of CO_2 and CH_4 [11]. CO_2 reforming can convert them to valuable chemicals. Secondly, it provides a good approach to utilize biogas and natural gas with a significant amount of CO_2 [12]. Thirdly, the highly endothermic nature of the reaction, which is even more endothermic than steam reforming of methane, makes it a good candidate for a chemical energy transmission system [1]. Finally, this reaction possesses a theoretical H_2/CO ratio of 1, which is suitable for further syntheses of hydrocarbons or oxygenated hydrocarbons:

$$CH_4 + CO_2 \rightarrow 2CO + 2H_2, \quad \Delta H = 247\,\text{kJ/mol}. \tag{1}$$

On the other hand, CO_2 reforming of methane is also accompanied by several side reactions: the reverse water gas shift reaction (RWGS (2)), the Boudouard reaction (3) and the methane decomposition (4). Reaction (2) consumes H_2 and CO_2 to produce additional CO, always resulting in a higher conversion of CO_2 than CH_4. Reactions (3) and (4) generate carbon deposits, which would destroy the catalyst particles and block the reactor, leading to the deactivation of catalyst. Considering that reaction (3) is exothermic while reaction (4) is endothermic, reaction (4) is more favored at high reaction temperatures [13,14]. In order to obtain high conversion, the reaction must be carried out at very high temperatures (>750 °C). Therefore, inhibition of coke formation from methane decomposition is of more practical importance.

$$H_2 + CO_2 \rightarrow H_2O + CO, \quad \Delta H = -39.5\,\text{kJ/mol}. \tag{2}$$

$$2CO \rightarrow CO_2 + C, \quad \Delta H = -171\,\text{kJ/mol}. \tag{3}$$

$$CH_4 \rightarrow 2H_2 + C, \quad \Delta H = 75\,\text{kJ/mol}. \tag{4}$$

It has been reported that noble metal-based catalysts (Rh, Ru, Ir and Pt) demonstrate high CO_2 reforming activity and high resistance to coking [7]. Nickel-based catalysts show

* Corresponding author. Fax: +86 22 27890078.
E-mail address: ughg_cjl@yahoo.com (C.-j. Liu).
[1] Present address: School of Chemical, Biological and Materials Engineering, The University of Oklahoma, Norman, OK 73019, USA.

0926-3373/$ – see front matter © 2007 Elsevier B.V. All rights reserved.
doi:10.1016/j.apcatb.2007.11.042

comparable activity with noble metal-based catalysts. However, nickel catalyst easily loses its activity due to the formation of coke. Because of the high cost and limited availability of noble metals, the development of a stable nickel-based catalyst is of great interest.

Many efforts have been made to develop coke free nickel catalysts. A general approach is selective blockage of part of the defect sites of Ni particle using inert element atoms. The inert element reported includes S [3], Sn [15], Au [16], and alkali and alkaline earth metal, such as K and Ca [17,18]. These element atoms are preferentially localized on the defect sites of Ni particle. The methane dissociation rate is moderately decreased, and thus a better carbon formation–gasification can be obtained, leading to a good coke inhibition property. This approach is usually accompanied by a decrease in activity.

Another approach reported is addition of active noble metal, for example, Ru, Rh and Pt, to the Ni catalysts to improve the coke resistance ability [19–22]. In contrast to the passivation with sulfur or the addition of alkali and alkaline earth metal, addition of noble metals improves the activity. It has been suggested that the formation of alloys [19,20] or an improvement of the nickel dispersion [21,22] is responsible for the improvements in activity and stability.

We previously demonstrated that the argon glow discharge treatment of Ni/Al_2O_3 followed by calcination thermally induces a significant enhancement in the anti-coke performance of the catalyst for CO_2 reforming [23]. Guo et al. [24] also confirmed that the treatment of Ni/Al_2O_3 catalyst using high frequency plasma favors the formation of small size Ni crystals and facilitates the high dispersion, leading to enhanced low-temperature activity and stability. In this work, we attempt to examine how the argon glow discharge plasma treatment affect the structure and reactivity of Ni/Al_2O_3 catalyst for CO_2 reforming of methane, with special attention paid to coke formation.

2. Experimental

2.1. Catalyst preparation

Two Ni/Al_2O_3 (W_{Ni}:$W_{alumina}$ = 5:100) catalysts were prepared by incipient wetness impregnation with and without plasma treatment. The γ-Al_2O_3 powder (provided by Institute of Chemical Engineering, Tianjin, S_{BET} = 230 m^2/g) was calcined at 600 °C for 4 h prior to use. It was impregnated for 12 h at room temperature with an aqueous solution of $Ni(NO_3)_2$, dried at 110 °C for 12 h, treated with argon glow discharge plasma and then calcined at 600 °C for 4 h. The obtained sample was referred to as NiAl-PC. The sample prepared without the plasma treatment was denoted as NiAl-C.

The plasma treatment was carried out at room temperature in an argon glow discharge system [25,26], as shown in Fig. 1. Catalyst powder (about 0.5 g) was loaded in a quartz boat and put into the discharge cell. After the pressure was adjusted in the range of 100–200 Pa, the discharge was initiated by applying voltage of 900 V to the electrode using a high voltage amplifier (Trek, 20/20B). The signal input for the high voltage amplifier was supplied by a function/arbitrary waveform generator (Hewlett Packard, 33120A) with a 100 Hz square wave. Ultrahigh pure grade argon (>99.999%) was used as the plasma-forming gas. During the plasma treatment, the surface of the sample turned from green to dark brown. The time of each plasma treatment was 10 min and each sample was treated for five times. Drops of water were added before the treatment to make the powder in better response to the discharges.

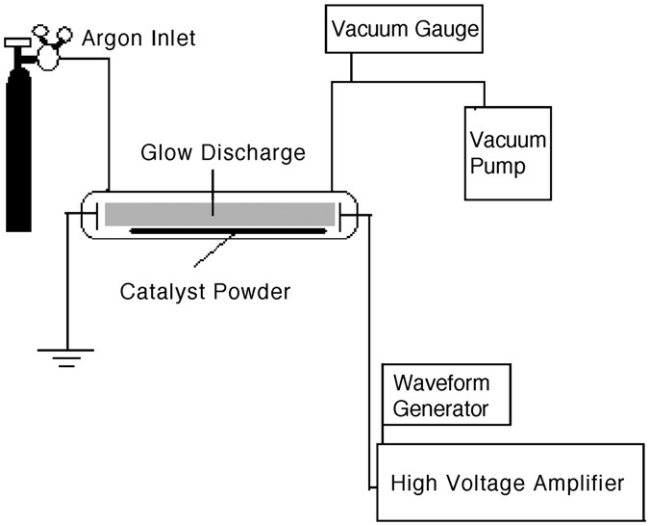

Fig. 1. Schematic representation of plasma treatment setup.

2.2. Characterizations

The specific surface area (BET) was measured by N_2 adsorption at −196 °C using a Quantachrome Autosorb-1 analyzer. The Ni content of the catalysts was measured by atomic absorption spectroscopy (AAS) using a Hitachi 180-80 atomic absorption spectrometer.

The X-ray powder diffraction (XRD) patterns of the catalyst samples were recorded by a Rigaku D/max-2500 diffractometer at a scanning speed of 4°/min over the 2θ range of 10–90°. The diffractometer was equipped with a Ni-filtered Cu Kα radiation source (λ = 1.54056 Å). The X-ray source was operated at 40 kV and 200 mA. The phase identification was made by comparison to Joint Committee on Powder Diffraction Standards (JCPDSs).

The X-ray photoelectron spectroscopy (XPS) study was conducted using a PHI-1600 system with Mg Kα radiation ($h\nu$ = 1253.6 eV). The Al 1s peak at 74.4 eV was used as an internal standard.

The hydrogen temperature programmed reduction (H_2-TPR) was carried out in a quartz micro-reactor, equipped with a flow control system, a temperature controller and a mass spectrometer (GSD301, Omnistar™). Approximately 150 mg of catalyst (40–60 mesh) was dried at 200 °C for 1 h in He (>99.999%, 30 cm^3/min). The temperature was then decreased to 50 °C, and 5% H_2/Ar (30 cm^3/min) was flowed through the sample for 30 min. Then the sample was heated at a rate of 10 °C/min to 1000 °C. The signals for H_2 (m/e = 2) and H_2O (m/e = 18) were recorded continuously.

Diffuse reflectance Fourier transform infrared (DRIFT) spectra were recorded on a Tensor 27 spectrometer (Bruker) equipped with a liquid nitrogen cooled Mercury–Cadmium–Tellurium (MCT) detector, a diffuse reflectance accessory (Praying Mantis, Harrick), and a high temperature reaction chamber (HVC, Harrick). The high temperature cell was fitted with two CaF_2 windows. The catalyst sample was firstly reduced *ex situ* at 700 °C for 2 h using flowing H_2. The catalyst powder (approximately 35 mg) was then loaded in the sample cup of the high temperature cell. The sample was reduced *in situ* at 300 °C for 1 h using flowing H_2 and then flushed with a flow of He for 30 min. The sample was then cooled to 25 °C. At this time, a background spectrum was recorded. 1.1 kPa of CO in He was flowed through the sample cup at 25 °C for 30 min. Then the cell was purged with flowing He for another 30 min. The spectrum was recorded with background spectrum subtracted at a resolution of 4 cm^{-1} and 64 scans.

An *in situ* temperature programmed oxidation (TPO) was then carried out using 3% O_2/He flow to evaluate the coke formed over the catalysts. The ramp rate was 10 °C/min. The products of CO_2 (m/z = 44) and CO (m/z = 28) were monitored by a mass spectrometer (GSD301, Omnistar™).

Transmission electron microscopy (TEM) observations were performed on a Philips TECNAI G^2F20 system equipped with an energy dispersion X-ray spectrometer (EDX) operated at 200 kV. The fine catalyst powder was dispersed ultrasonically in ethanol. A drop of the suspension was deposited on a carbon coated copper grid for TEM analysis.

2.3. Activity test

Catalytic performance was carried out in a quartz tube with an inner diameter of 4 mm at ambient pressure. A catalyst sample of 50 mg (40–60 mesh) was packed in the quartz tube with two layers of quartz wool. It was reduced *in situ* by 20 cm^3/min flowing H_2 at 700 °C for 2 h. Then the temperature was decreased to 500 °C in flowing Ar. The feed gases of CH_4 and CO_2 diluted in Ar (1:1:2) were introduced into the micro-reactor by mass flow controllers. The reaction temperature was increased to 800 °C in a step-wise fashion. The gas hourly space velocity (GHSV) was 4.8×10^4 $cm^3/(g_{cat}\ h)$. The feed gases were ultra high pure grade (>99.999%), which were used without further purification. The gas residue was analyzed online by a gas chromatograph (GC, Agilent 6890) equipped with a thermal conductivity detector (TCD) and a 2-m TDX-01 packed column, using Ar as the carrier gas. An ice trap was placed between the outlet of the reactor and the GC to remove water. For the stability test, the temperature was increased to 750 °C in flowing Ar immediately after the sample was reduced in flowing H_2 for 2 h at 700 °C.

3. Results

3.1. Characterizations

3.1.1. BET and AAS

The fresh samples of NiAl-C and NiAl-PC have similar BET surface area, as shown in Table 1. After 6 h reaction, the BET surface area reduced, as a result of both Al_2O_3 sintering and coke formation. The Ni contents of both samples measured by AAS are essentially identical, very close to the nominal Ni content (4.7%).

Table 1
BET surface areas and AAS Ni contents

Sample	BET surface area (m^2/g)		AAS Ni content (wt%)
	Fresh	Used[a]	
NiAl-C	206	164	4.55
NiAl-PC	205	170	4.51

[a] After 6 h reaction from 500 to 800 °C.

3.1.2. XRD

The XRD patterns for the γ-Al_2O_3 support (a), the fresh NiAl-C (b) and NiAl-PC (c) catalysts, as well as the reduced NiAl-C (d) and NiAl-PC (e) samples are shown in Fig. 2. The XRD patterns for the first three samples are very similar (Fig. 2a–c), with γ-Al_2O_3 phase present principally. However, a careful examination of the two fresh samples reveals that there is an intensity increase at the 2θ values slightly lower than the 2θ of the γ-Al_2O_3 peak. This indicates that nickel aluminate spinel ($NiAl_2O_4$) is formed in the two samples. It has been reported that γ-Al_2O_3 has a pseudospinel structure and its lattice parameters are very close to that of $NiAl_2O_4$, with 2θ shifted slightly to higher values [27].

After reduction at 700 °C for 2 h, nickel (1 1 1), (2 0 0) and (2 2 0) faces are clearly visible at 2θ of 44.5°, 51.8° and 76.4°, respectively (Fig. 2d and e). The average particle sizes of Ni, estimated by Scherrer formula using full width at half maximum of Ni (2 0 0), are 10.1 and 7.3 nm for the reduced NiAl-C and NiAl-PC samples, respectively. The estimated percent dispersion ($D\% = 100/d_{XRD}$ [9]) is 9.9 and 13.7% for the NiAl-C and NiAl-PC, respectively. The plasma treatment generates smaller Ni particles with higher dispersion.

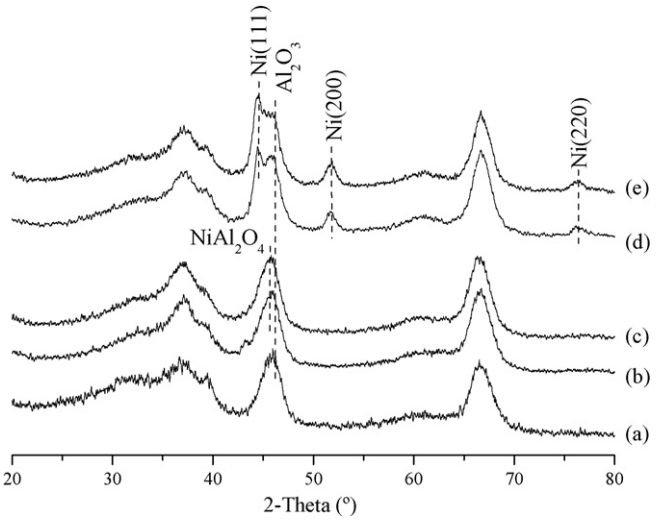

Fig. 2. XRD patterns of (a) γ-Al_2O_3; (b) NiAl-C; (c) NiAl-PC; (d) NiAl-C reduced at 700 °C for 2 h; (e) NiAl-PC reduced at 700 °C for 2 h.

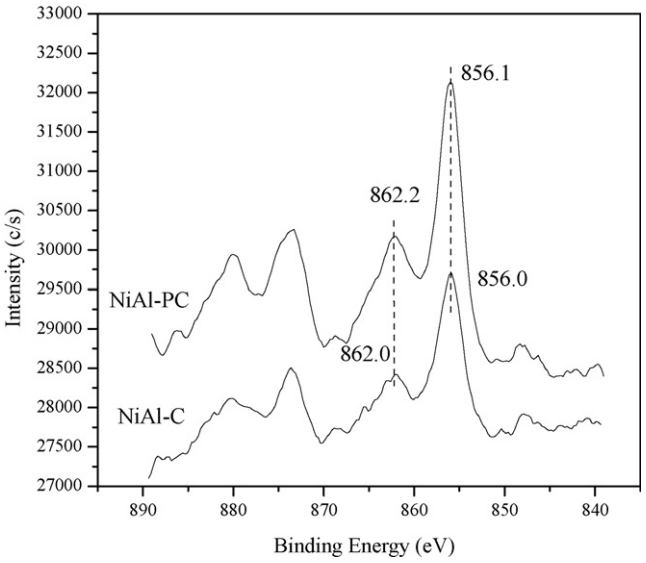

Fig. 3. XPS spectra of fresh NiAl-C and NiAl-PC samples in the Ni 2p region.

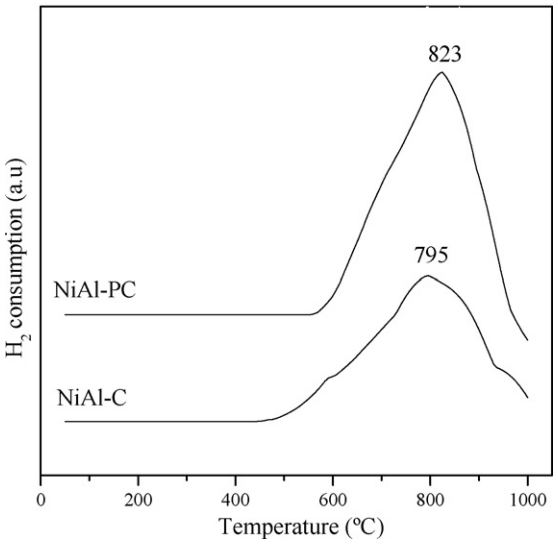

Fig. 4. H_2-TPR profiles of NiAl-C and NiAl-PC samples.

3.1.3. XPS

The XPS spectra of the Ni 2p region of the fresh calcined NiAl-C and NiAl-PC samples are shown in Fig. 3. The Ni $2p_{3/2}$ peak at binding energy of 856.0 eV is accompanied by a shake-up satellite peak at 862.0 eV in the NiAl-C sample. This peak can be assigned to $NiAl_2O_4$ species [13]. The $NiAl_2O_4$ peak is also observed for the NiAl-PC sample. The intensity of the Ni $2p_{3/2}$ peak of the NiAl-PC sample is significantly higher than that for NiAl-C. The Ni/Al ratios estimated from XPS analyses are 0.039 and 0.069 for NiAl-C and NiAl-PC, respectively. If it is assumed that the Ni species are 100% dispersed in the Al_2O_3, the nominal Ni/Al ratio will be 0.044. Obviously, the Ni/Al ratio of the NiAl-PC sample is much higher than the nominal ratio. Because the Ni loading contents of the two samples are essentially the same (as shown in Table 1), the higher Ni/Al ratio suggests that the plasma treatment induces an enrichment of Ni species on the alumina surface. This result is in line with our previous work that confirms plasma treatment enriches the PdO on the zeolite surface [25].

3.1.4. H_2-TPR

H_2-TPR is usually used to characterize the interaction between the support and the supported species. Small NiO particles strongly bonded to the support is normally reduced at higher temperatures than large particles with poor metal–support interaction. The H_2-TPR profiles of NiAl-C and NiAl-PC are exhibited in Fig. 4. Both samples show only one reduction peak. The reduction peak for NiAl-C is at 795 °C, and for NiAl-PC it is 823 °C. In general, three types of Ni species can exist over Al_2O_3: bulk or free NiO (reduction temperature <400 °C); NiO bonded to Al_2O_3 (reduction temperature 400–690 °C); and NiO incorporated into Al_2O_3, i.e., formation of $NiAl_2O_4$ (reduction temperature >700 °C, with the maximum reduction temperature in the range of 780–830 °C) [28]. Thus, it can be concluded that $NiAl_2O_4$ is present in both samples, and the Ni species interacts with Al_2O_3 more strongly in the NiAl-PC sample. The verification of formation of $NiAl_2O_4$ by H_2-TPR is in agreement with XRD and XPS results. It should be also noted that the reduction peak of NiAl-PC is more symmetric than that of NiAl-C, indicating that the Ni species distribution is more homogenous in the NiAl-PC sample.

3.1.5. CO adsorbed DRIFT

Fig. 5 shows the DRIFT spectra of CO adsorbed on reduced NiAl-C and NiAl-PC at 25 °C. The high frequency band at 2100–2000 cm^{-1} can be assigned to linearly adsorbed CO on Ni^0; the low frequency band at 2000–1750 cm^{-1} is attributed to two- or three-fold bridge adsorbed CO on Ni^0 [19,20,22,29–33]. The linearly adsorbed CO is centered at 2062 and 2067 cm^{-1} for NiAl-PC and NiAl-C, respectively. This red shift of linear CO band for NiAl-PC with regard to that for NiAl-C can be related to the smaller particles for NiAl-PC,

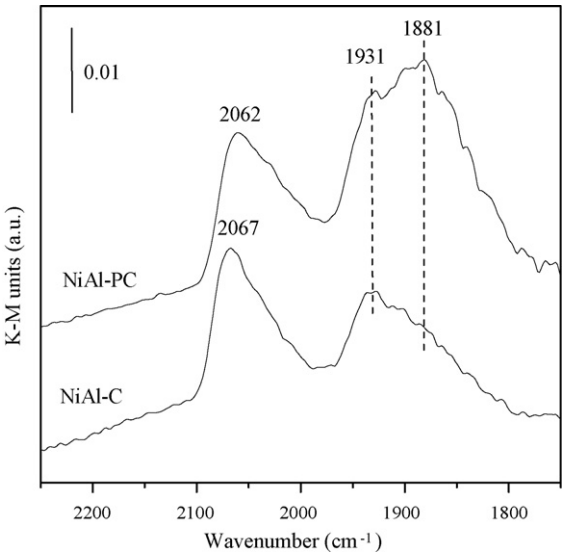

Fig. 5. DRIFT spectra of CO adsorbed on reduced NiAl-C and NiAl-PC samples. Spectra were recorded after sample exposed to 1.1 kPa CO in He for 30 min, and He flow for another 30 min.

since smaller particle gives a stronger back donation [29]. The two-fold bridge adsorbed CO band at 1931 cm^{-1} is observed for both samples. Another band at 1881 cm^{-1} is only present for the NiAl-PC, which can be ascribed to three-fold bridge adsorbed CO. Geometrically, CO preferentially bonds linearly to defect sites, whereas bridged bonding (two- or three-fold) is more favorable at close packed plane sites [31–33]. Therefore, different linearly to bridge (L/B) adsorbed CO ratio indicates different concentration of defect sites and close packed planes. The L/B ratios are 0.91 and 0.47 for NiAl-C and NiAl-PC, respectively. As detailed discussed elsewhere [34], the decrease of L/B ratio of NiAl-PC with respect to NiAl-C is not related to increasing Ni particle size but to the changes in morphology, i.e., the increase of close packed plane concentration of Ni particle for NiAl-PC (or smoothening the surface of Ni particle).

3.2. Reactivity

The activity tests of the NiAl-C and NiAl-PC samples were performed as a function of reaction temperature, as exhibited in Fig. 6. For both samples, CH_4 and CO_2 conversions increase with increasing temperatures. The conversions of both CH_4 and CO_2 are 4–7% higher over the NiAl-PC catalyst in the reaction temperature range of 500 to 800 °C. The H_2/CO ratio is also higher for the NiAl-PC sample. The high activity of the NiAl-PC sample is probably due to its higher dispersion. It should be noted that, for both samples, the conversion of CO_2 is always higher than that of CH_4, because of the RWGS reaction (2) [35]. The H_2/CO ratio increases with increasing temperatures, as the RWGS reaction becomes less favored.

The NiAl-PC sample was tested for 50 h time on stream at 750 °C and the results are shown in Fig. 7. The sample is very stable without deactivation for either CH_4 or CO_2 conversion. For the NiAl-C sample, the conversion of CH_4 is declined slightly during 10 h time on stream tested. The results for the NiAl-C are consistent with Wang and Lu [36].

TEM analyses were carried out to observe the changes in Ni particle size and coke formation. The TEM images of the NiAl-C sample obtained after 10 h time on stream at 750 °C are shown in Fig. 8. Most of the Ni particles are smaller than 20 nm. Some large particles up to 40 nm can also be observed (Fig. 8a). In some cases, filamentous carbon with Ni particle (marked with an arrow) on the tip can be observed (Fig. 8b). Larger particles are clearly more easily to be coked with filamentous carbon. However, filamentous carbon with diameters smaller than 10 nm can be observed too (Fig. 8c). Encapsulating carbon is also observed in some cases. An example of encapsulating carbon is shown in Fig. 8d. From this figure, a Ni particle about 14 nm surrounded by layers of graphitic carbon can be observed.

For the NiAl-PC sample, after 50 h time on stream at 750 °C, no obvious filamentous carbon or encapsulating carbon can be observed even with careful examination (Fig. 9a). Although their presence cannot be absolutely ruled out due to the limitation of TEM observations, the TEM results do suggest that the filamentous carbon and encapsulating carbon are greatly suppressed in the NiAl-PC sample. A typical EDX spectrum of the Ni particle is shown in Fig. 9b. It is clear that the particle contains some carbon. The very low C/Ni ratio indicates the carbon is most probably in the Ni_3C form and locates on the Ni particle surface. It is well known that carbon can dissolve in Ni particles to form Ni_3C, which has been suggested by some authors as the active phase for CO_2 reforming of methane [37].

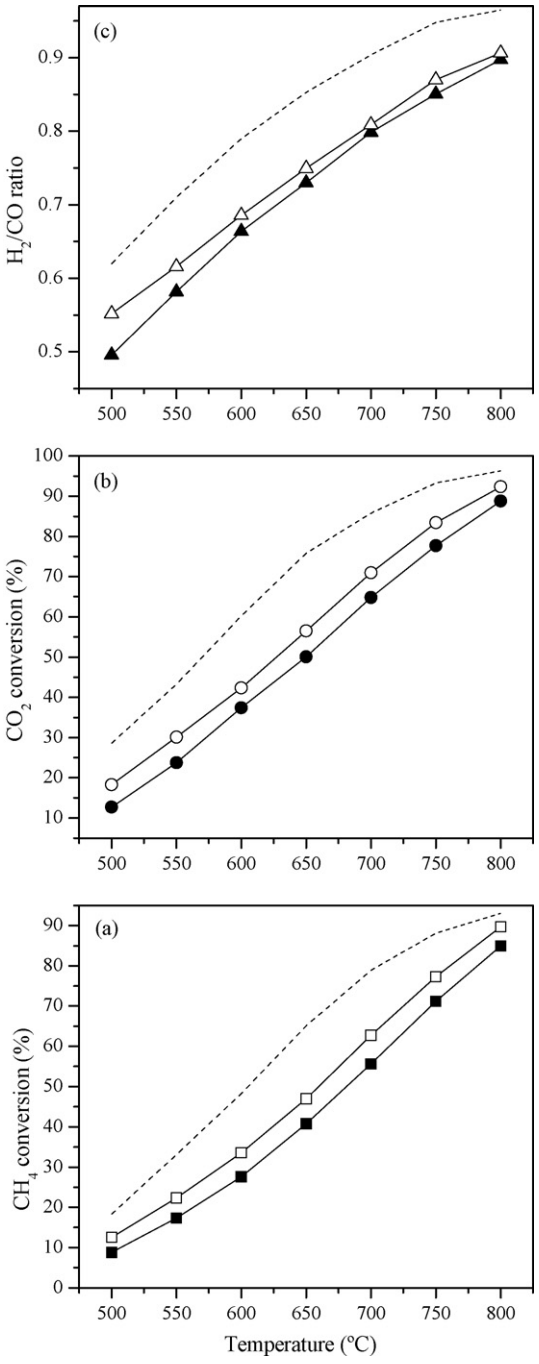

Fig. 6. Effect of reaction temperature on (a) CH_4 conversion, (b) CO_2 conversion, and (c) H_2/CO ratio of NiAl-C (filled symbols), NiAl-PC (open symbols) samples, and thermodynamic equilibrium data of CO_2 reforming and reverse water gas shift (dash line). Reaction conditions: 50 mg, GHSV = 4.8×10^4 $cm^3/(g_{cat}\ h)$, CH_4:CO_2:Ar = 1:1:2, pressure = 1 atm.

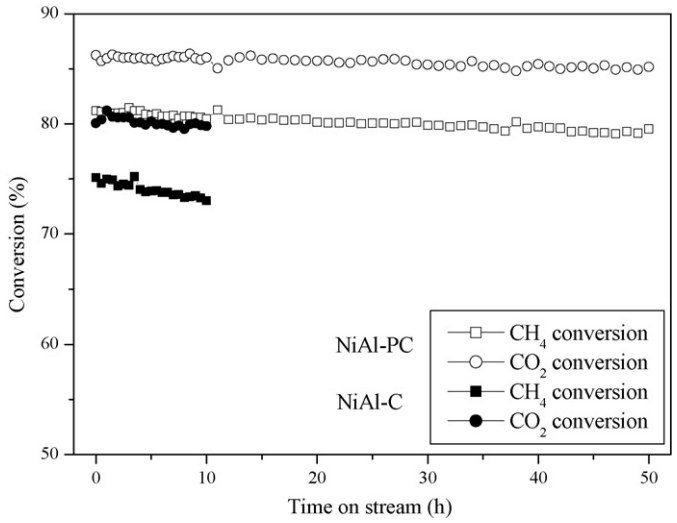

Fig. 7. Stability tests of NiAl-C (filled symbols) and NiAl-PC (open symbols) samples. Reaction conditions: $T = 750\ ^{\circ}C$, 50 mg, GHSV = $4.8 \times 10^4\ cm^3/(g_{cat}\ h)$, CH_4:CO_2:Ar = 1:1:2, pressure = 1 atm.

Fig. 10 compares the particle size distribution obtained from TEM images of the NiAl-C sample after 10 h time on stream and the NiAl-PC sample after 50 h time on stream at 750 °C. For the NiAl-C sample, there is a broad range of particle size up to near 40 nm. In contrast, the particle size distribution is much narrower for the NiAl-PC, with the largest particle smaller than 20 nm. The number-weighted particle size, d_n, is 12.0 and 7.4 nm for NiAl-C and NiAl-PC, respectively, which is in line with the average particle size estimated from the XRD of the fresh samples reduced at 700 °C. These results indicate that, for both samples, sintering occurred only to a limited extent, although the reaction temperature is much higher than the Tammann temperature (590 °C for Ni, above which Ni sintering is possible [38]).

An *in situ* TPO was carried out to evaluate the coke formed after 5 h time on stream at 750 °C, as shown in Fig. 11. It is generally accepted that several kinds of carbon exists in the Ni catalyst: very active monatomic carbon, filamentous carbon and encapsulating carbon, and amorphous and/or graphitic carbon deposited on the support [21,38–40]. Filamentous carbon has no effect on the activity of the catalyst, but large amounts of it

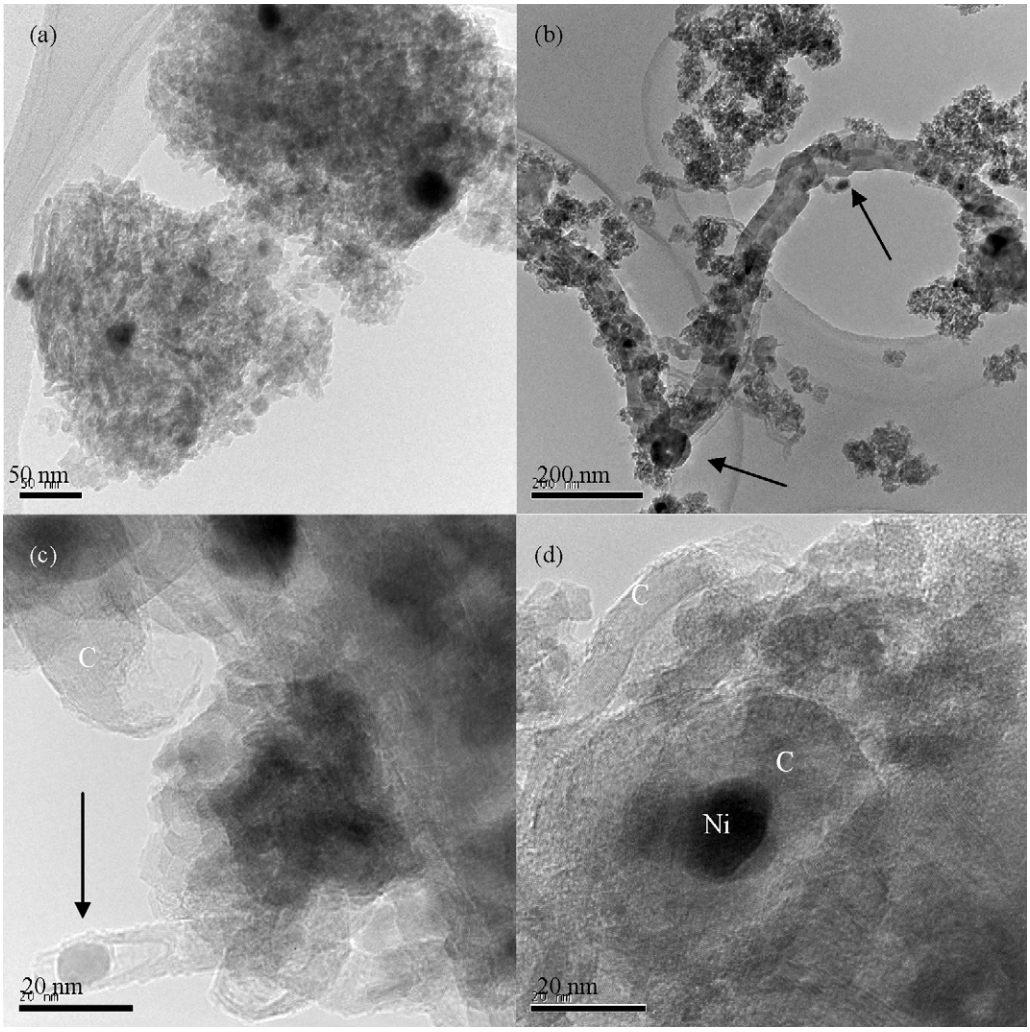

Fig. 8. TEM images NiAl-C sample after 10 h time on stream at 750 °C: (a) an overview of particle size distribution; (b) an example of filamentous carbon; (c) another example of filamentous carbon; (d) an example of encapsulating carbon.

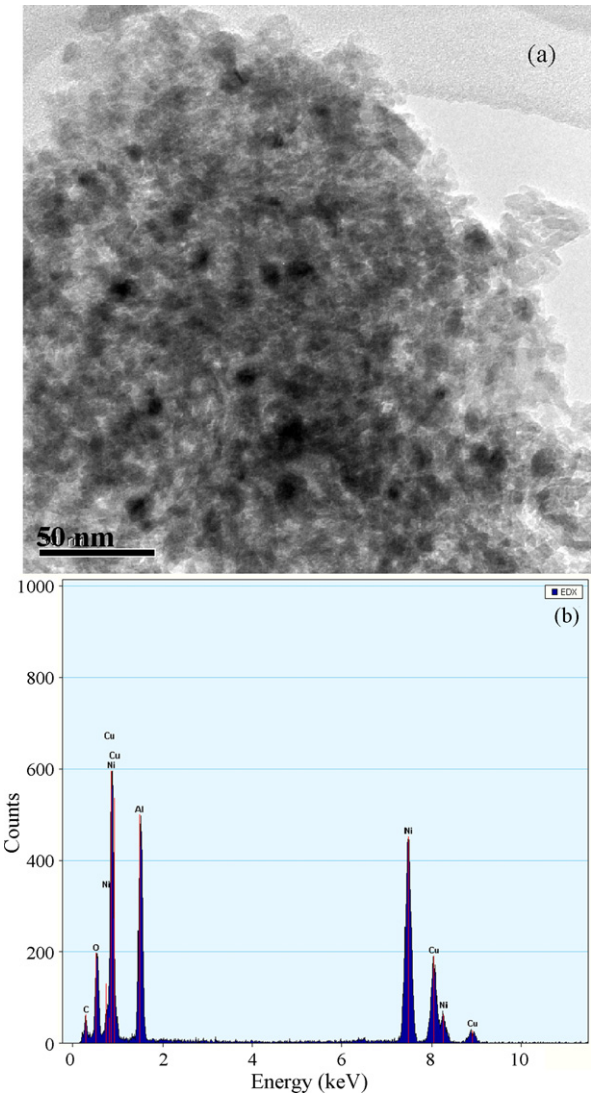

Fig. 9. TEM images of NiAl-PC sample after 50 h time on stream at 750 °C: (a) an overview of particle size distribution; (b) EDX of a Ni particle.

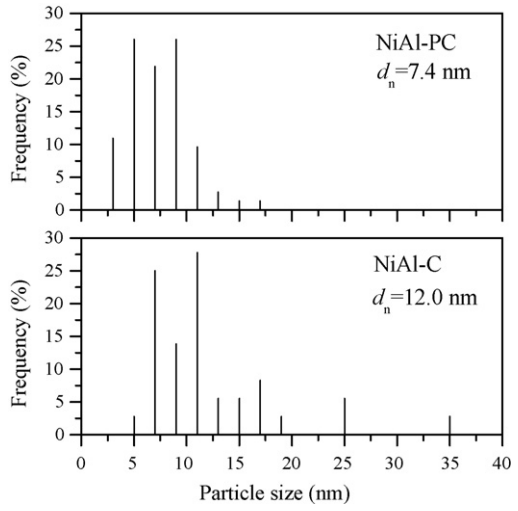

Fig. 10. Particle size distributions of NiAl-C after 10 h time on stream and NiAl-PC after 50 h time on stream at 750 °C. Number-weighted particle size: $d_n = \Sigma n_i d_i / \Sigma n_i$ [35].

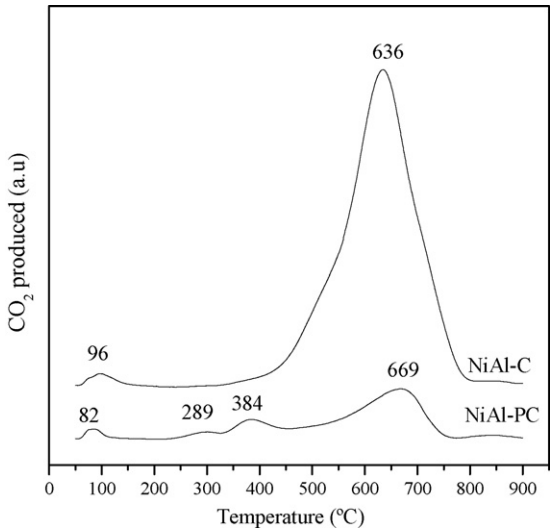

Fig. 11. TPO profiles of NiAl-C and NiAl-PC after 5 h time on stream at 750 °C. Reaction conditions are the same with Fig. 7.

destroy the catalyst particles and plug the reactor for a long-term run. Encapsulating carbon is responsible for the deactivation of the catalyst. The TPO profile for the NiAl-C sample shows a small CO_2 peak at 96 °C and an intense peak at 636 °C. The high temperature peak is very broad, starting at 310 °C and ending at 817 °C, indicating that it contains different types of carbon species. For the NiAl-PC sample, three main peaks centered at 82, 384, and 669 °C as well as a very weak peak at 289 °C are present. Carbon species oxidized at lower than 100 °C can be assigned to reactive monatomic carbon, which is the intermediate of the reaction [35,39]. For the NiAl-PC sample, the peaks at 289 and 384 °C can be attributed to Ni_3C, and the peak at 669 °C is probably generated from the amorphous carbon on the support. For the NiAl-C sample, the broad peak at 636 °C can be assigned to a combined contribution from Ni_3C, filamentous carbon, encapsulating carbon, and carbon on the support. The TPO profile of the NiAl-C sample is very similar to the reported TPO profile of Ni/γ-Al_2O_3 [36]. The amount of coke formed over NiAl-C and NiAl-PC are 0.413 and 0.0829 mmol carbon/g_{cat}, respectively. Combined with the results of TEM and TPO, it can be concluded that the formation of filamentous and encapsulating carbon are greatly inhibited for the NiAl-PC sample.

4. Discussion

Based on the characterization results, we propose the structure models for the NiAl-C and NiAl-PC samples, as illustrated in Fig. 12a and b, respectively, for CO_2 reforming of methane. For the NiAl-C sample, the spherical Ni particles (rough surface with higher concentration of defect sites) contact the support with a smaller interface. For the NiAl-PC sample, smoothened Ni particles are spread over the alumina support with a larger contacting interface. With this model, the results of TPR, CO adsorbed DRIFT and XPS can be easily explained. Because of polycrystalline property of the Al_2O_3, the interface of Ni-Al_2O_3 was not directly observed in this study. In fact, this

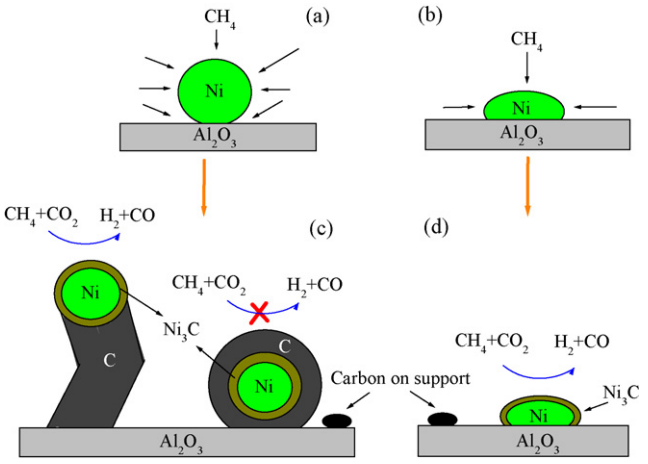

Fig. 12. Schematic representation of CO_2/CH_4 reforming over (a and c) NiAl-C; and (b and d) NiAl-PC samples.

model is in line with the TEM observations in our previous work [41]. In that case, a clear interface of Ni–ZrO_2 and Ni–Ta_2O_3 were observed by TEM. And those plasma treated samples showed flatter morphology. Therefore, it is reasonable to assume that the NiAl-PC sample has a flat morphology and a larger interface.

Coke formation over Ni surfaces is well understood except for a few details, which are still under debate [38,42,43]. It is considered that methane dissociates over the surface to form very active monatomic carbon. If the rate of the monatomic carbon gasification by CO_2 is less than the rate of monatomic carbon formation, the carbon will polymerize. The polymerized carbon may accumulate on the surface or dissolve in the Ni particles. The accumulation of surface carbon encapsulates the Ni particles to form encapsulating carbon; while the dissolved carbon diffuses through the Ni particle (bulk or surface diffuse) to the Ni–support interface and lifts the Ni particle away from the support to form filamentous carbon. Therefore, the coke formation is determined by the balance of carbon formation–gasification. It is well known that decomposition of methane is structure sensitive, with higher activation energy over close packed planes (i.e., high coordinated sites, such as Ni(1 1 1)) than that over defect sites or open planes (i.e., low coordinated sites, such as Ni(1 0 0)) [8,44,45]. The rate of methane decomposition on different sites of Ni will significantly influence the balance of carbon formation–gasification.

The NiAl-C sample contains a higher concentration of defect sites, and has weaker metal–support interactions. Methane is expected to be dissociated from all directions of the Ni particle [37]. Methane dissociation is faster on these defect sites [37,44,45], forming a larger amount of graphene. The graphene nucleates quickly on the surface of Ni to form encapsulating carbon [37]. It may also dissolve in the Ni and diffuse through it to detach the Ni particles from the support, forming filamentous carbon. In the case of filamentous carbon, CO_2 reforming can still take place on the Ni located on the tip of carbon filament. However, for the encapsulating carbon, CH_4 and CO_2 do not have access to Ni, and hence the reaction is ceased. The schematic representation is shown in Fig. 12c.

The NiAl-PC sample contains higher portion of close packed plane (i.e., smoothened Ni surface, confirmed by CO adsorbed DRIFT results), with which methane is expected to be dissociated from limited directions. The rate of methane dissociation on the close packed planes is less than that over the defect sites [37,44,45]. Therefore, the produced carbon can be more quickly removed by CO_2 to form CO, resulting in a better carbon formation–gasification balance. Furthermore, the particle size of NiAl-PC is smaller than that of NiAl-C, so that the driving force for the carbon dissociation at the Ni and diffusion through it will be smaller [46]. In addition, the metal–support interaction is stronger for NiAl-PC sample, as shown in Fig. 4. It is therefore more difficult for the carbon to lift the Ni particle from the support [42]. The schematic representation is shown in Fig. 12d. As a consequence, the formation of both filamentous carbon and encapsulating carbon is greatly suppressed, as supported by TPO results and TEM observations.

The lower methane decomposition rate over the NiAl-PC can be further demonstrated if we compare the turnover frequency (TOF) of methane, defined as methane converted per surface Ni atom per second. For example, the TOF at 750 °C is 1.48 and 1.02 s^{-1} for NiAl-C and NiAl-PC, respectively [34]. The moderately decrease in methane dissociation rate over NiAl-PC will produce a lower amount of carbon, which can be quickly removed by CO_2. Therefore, a better balance of carbon formation from methane decomposition and carbon gasification by CO_2 can be obtained over the NiAl-PC sample, leading to a better anti-coke performance.

5. Conclusion

The Ni/Al_2O_3 catalyst prepared by plasma treatment followed by calcination thermally shows improved activity and stability with respect to the un-treated sample. XRD and TEM results show that the plasma treated sample has smaller Ni particle size than the sample prepared without plasma treatment. In addition, the particle size distribution is also narrower for the plasma treated sample. H_2-TPR results reveal a stronger interaction between the Ni and the alumina for the plasma treated sample. CO adsorbed DRIFT results suggest smoothening of Ni particle surface for the plasma treated sample compared with the un-treated sample. The smaller Ni particle size (with higher dispersion) provides more active sites for reaction, leading to higher conversions of CH_4 and CO_2. In addition, smoothened Ni particle moderately reduces the specific rate of methane decomposition, resulting in a better balance of carbon formation–gasification. The anti-coke formation ability is thereby improved. Moreover, the stronger interaction of Ni–support of the plasma treated sample also inhibits the coke formation.

Acknowledgments

The supports from National Natural Science Foundation of China (under contract 20490203) and 973 project (under contract 2005CB221406) are greatly appreciated. The instru-

ment supports from ABB Switzerland and from the Program for Changjiang Scholars and Innovative Research Team from the Ministry of Education of China are also appreciated.

References

[1] A.M. Gadalla, B. Bower, Chem. Eng. Sci. 43 (1988) 3049–3062.
[2] D.A. Slade, A.M. Duncan, K.J. Nordheden, S.M. Stagg-Williams, Green Chem. 9 (2007) 577–581.
[3] J.R. Rostrup-Nielsen, J.-H.B. Hansen, J. Catal. 144 (1993) 38–49.
[4] N. Laosiripojana, S. Assabumrungrat, Appl. Catal. B 60 (2005) 107–116.
[5] A.M. O'Conor, Y. Schuurman, J.R.H. Ross, C. Mirodatos, Catal. Today 115 (2006) 191–198.
[6] M.C.J. Bradford, M.A. Vannice, Catal. Rev. Sci. Eng. 41 (1999) 1–42.
[7] Y.H. Hu, E. Ruckenstein, Adv. Catal. 48 (2004) 297–345.
[8] T.V. Choudhary, D.W. Goodman, J. Mol. Catal. A 163 (2000) 9–18.
[9] J.M. Wei, E. Iglesia, J. Catal. 224 (2004) 370–383.
[10] H. Sun, H. Wang, J. Zhang, Appl. Catal. B 73 (2007) 158–165.
[11] B. Delmon, Appl. Catal. B 1 (1992) 139–147.
[12] F. Pompeo, N.N. Nichio, M.G. González, M. Montes, Catal. Today 107–108 (2005) 856–862.
[13] D. Dissanayake, M.P. Rosynek, K.C.C. Kharas, J.H. Lunsford, J. Catal. 132 (1991) 117–127.
[14] S.S. Bharadwaj, L.D. Schmidt, J. Catal. 146 (1994) 11–21.
[15] E. Nikolla, A. Holewinski, J. Schwank, S. Linic, J. Am. Chem. Soc. 128 (2006) 11354–11355.
[16] F. Besenbacher, I. Chorkendorff, B.S. Clausen, B. Hammer, A.M. Moelenbroek, J.K. Nørskov, I. Steensgaard, Science 279 (1998) 1913–1915.
[17] T. Osaki, T. Mori, J. Catal. 204 (2001) 89–97.
[18] J. Juan-Juan, M.C. Román-Martínez, M.J. Illán-Gómez, Appl. Catal. A 301 (2006) 9–15.
[19] C. Crisafulli, S. Scirè, R. Maggiore, S. Minicò, S. Galvagno, Catal. Lett. 59 (1999) 21–26.
[20] C. Crisafulli, S. Scirè, S. Minicò, L. Solarino, Appl. Catal. A 225 (2002) 1–9.
[21] Z.Y. Hou, T. Yashima, Catal. Lett. 89 (2003) 193–197.
[22] J.A.C. Dias, J.M. Assaf, J. Power Sources 130 (2004) 106–110.
[23] D.G. Cheng, X.L. Zhu, Y.H. Ben, F. He, L. Cui, C.J. Liu, Catal. Today 115 (2006) 205–210.
[24] F. Guo, W. Chu, H. Xu, T. Zhang, Chin. J. Catal. 28 (2007) 429–434.
[25] C.J. Liu, K.L. Yu, Y.P. Zhang, X.L. Zhu, F. He, B. Eliasson, Appl. Catal. B 47 (2004) 95–100.
[26] X.L. Zhu, P.P. Huo, Y.P. Zhang, C.J. Liu, Ind. Eng. Chem. Res. 45 (2006) 8604–8609.
[27] M.L. Jacono, M. Schiavello, A. Cinico, J. Phys. Chem. 75 (1972) 1044–1050.
[28] J.M. Rynkowski, T. Paryjczak, M. Lenik, Appl. Catal. A 106 (1993) 73–82.
[29] G. Blyholder, J. Phys. Chem. 68 (1964) 2772–2777.
[30] C.H. Rochester, R.J. Terrell, J. Chem. Soc. Faraday Trans. I 73 (1977) 609–621.
[31] D.G. Blackmond, E.I. Ko, J. Catal. 96 (1985) 210–221.
[32] J.A. Anderson, M.T. Rodrigo, L. Daza, S. Mendioroz, Langmuir 9 (1993) 2485–2490.
[33] A.F.H. Wielers, G.J.M. Aaftink, J.W. Geus, Appl. Surf. Sci. 20 (1985) 564–580.
[34] X.L. Zhu, Y.P. Zhang, C.J. Liu, Catal. Lett. 118 (2007) 306–312.
[35] M.C.J. Bradford, M.A. Vannice, Appl. Catal. A 142 (1996) 73–96.
[36] S.B. Wang, G.Q.M. Lu, Appl. Catal. B 16 (1998) 269–277.
[37] V.C.H. Kroll, H.M. Swaan, C. Mirodatos, J. Catal. 161 (1996) 409–422.
[38] D.L. Trimm, Catal. Today 49 (1999) 3–10.
[39] Z.L. Zhang, X.E. Verykios, Catal. Today 21 (1994) 589–595.
[40] L. Kepinski, B. Stasinska, T. Borowiecki, Carbon 38 (2000) 1845–1856.
[41] J.-J. Zou, C.-J. Liu, Y.-P. Zhang, Langmuir 22 (2006) 2334–2339.
[42] R.T.K. Baker, Carbon 27 (1989) 315–323.
[43] I. Alstrup, J. Catal. 109 (1988) 241–251.
[44] H. Burghgraef, A.P.J. Jansen, R.A.V. Santen, Surf. Sci. 324 (1995) 345–356.
[45] J.R. Rostrup-Nielsen, J.K. Nørskov, Top. Catal. 40 (2006) 45–48.
[46] D. Chen, K.O. Christensen, E. Ochoa-Fernández, Z.X. Yu, B. Tøtdal, N. Latorre, A. Monzón, A. Holmen, J. Catal. 229 (2005) 82–96.